Journal of Computational Physics **148,** 133–148 (1999)
Article ID jcph.1998.6108, available online at http://www.idealibrary.com on IDEAL®

# Maintaining Pressure Positivity in Magnetohydrodynamic Simulations

Dinshaw S. Balsara* and Daniel Spicer†

**N.C.S.A., University of Illinois at Urbana Champaign, Urbana, Illinois 61801;*
†*Code 930, NASA/GSFC, Greenbelt, Maryland 20771*
E-mail: dbalsara@ncsa.uiuc.edu, spicer@gauss.gsfc.nasa.gov

Received January 27, 1998; revised September 8, 1998

Higher order Godunov schemes for solving the equations of magnetohydrodynamics (MHD) have recently become available. Because such schemes update the total energy, the pressure is a derived variable. In several problems in laboratory physics, magnetospheric physics, and astrophysics the pressure can be several orders of magnitude smaller than either the kinetic energy or the magnetic energy. Thus small discretization errors in the total energy can produce situations where the gas pressure can become negative. In this paper we design a linearized Riemann solver that works directly on the entropy density equation. We also design switches that allow us to use such a Riemann solver safely in conjunction with a normal Riemann solver for MHD. This allows us to reduce the discretization errors in the evaluation of the pressure variable. As a result we formulate strategies that maintain the positivity of pressure in all circumstances. We also show via test problems that the strategies designed here work. 

## 1. INTRODUCTION

When the equations of magnetohydrodynamics (MHD) are written in conservative form the pressure, $P$, is a variable whose value has to be derived at each timestep. In order to derive the value of the pressure one has to subtract off the kinetic energy $\rho\mathbf{v}^2/2$ and magnetic energy $\mathbf{B}^2/8\pi$ from the total energy $E = \rho\mathbf{v}^2/2 + \mathbf{P}/(\gamma - 1) + \mathbf{B}^2/8\pi$, where $\gamma$ is the ratio of specific heats. Often these can be quite large relative to the value of the pressure. For example, $\beta = 8\pi P/\mathbf{B}^2 \preceq 10^{-4}$ are quite common in both stellar atmospheres such as the Sun's and in the Earth's magnetosphere. Thus discretization errors made in computing the total energy and the kinetic energy and magnetic energies can be large enough to result in negative pressure. This results in an unacceptable physical situation in the computation of MHD flows. In all the computational situations where the pathology occurs one notices that the local fluid flow in regions where $\beta$ is small, is typically adiabatic,



0021-9991/99 $30.00

and there are no magnetosonic shocks. In the vicinity of shocks, as long as the magneto-fluid has a positive pressure in the region in front of the magnetosonic shock, the fluid behind the magnetosonic shock will have positive pressure, owing to the fact that magnetosonic shocks are compressive. The only other MHD discontinuities where the fluid actually passes through the discontinuity are Alfvén waves. When a parcel of fluid passes through a torsional Alfvén wave discontinuity its entropy is preserved. Entropy waves in MHD, just like the entropy waves in the Euler equations, do not allow the fluid to pass through the discontinuity. The negative pressure is, therefore, simply produced (in regions without magnetosonic shocks) because we subtract two large numbers, that is, the kinetic energy and the magnetic energy, from a third large number, the total energy. As long as the zones in front of a magnetosonic shock have positive pressure, negative pressures would not be produced in magnetosonic shocks.

A similar problem arises in the modelling of high speed fluid flows with the Euler equations. In that case two solution strategies become possible. The first, suggested by Ryu *et al.* [1], consists of using a modified entropy equation written in conservation form instead of using the total energy equation to complete the hyperbolic system. We draw on that strategy here in formulating a method for preserving pressure positivity in MHD flows. The second strategy, suggested by Linde and Roe [2] relies on two facts: (a) the fluxes of the Euler system are first-order functions of the conserved variables and (b) a Riemann solver exists which always produces a positive pressure at the zone boundary. For the Euler equations the Riemann solver of choice, as suggested by Linde and Roe [2], is the exact Riemann solver for the Euler equations. Such an exact Riemann solver for the Euler equations has been formulated by vanLeer [3]. It is important to note that, even in the method of Linde and Roe [2], the use of the exact Riemann solver alone cannot fix the problem completely. The reason is that discretization errors in the monotonicity-preserving reconstruction, as well as in the flux differencing can reduce the accuracy with which the total energy is evolved and thereby cause the pressure to become negative in certain situations in a low $\beta$ flow. For MHD the fluxes are not a first-order function of the conserved variables. Also an exact Riemann solver for MHD is difficult to formulate and takes up far too much computational time to be usable in any real numerical scheme. For this reason we draw on the first strategy in this paper, rather than the second. The method developed here is general in that it would apply to other schemes that use different monotonicity-preserving interpolation strategies. It is also general in that any other linearized Riemann solver can also be reformulated using the ideas developed here so that the resultant scheme guarantees pressure positivity.

In Section 2 we outline our numerical strategy for ensuring pressure positivity. In Section 3 we give some numerical examples. In Section 4 we arrive at some conclusions.

## 2. THE NUMERICAL STRATEGY

The method consists of realizing that the entropy equation

$$\frac{\partial}{\partial t}\left(\frac{P}{\rho^\gamma}\right) + \mathbf{v}\cdot\boldsymbol{\nabla}\left(\frac{P}{\rho^\gamma}\right) = 0 \tag{1}$$

can be coupled with the continuity equation to derive a conservative equation for the entropy

density which can be written as

$$\frac{\partial}{\partial t}\left(\frac{P}{\rho^{\gamma-1}}\right)+\boldsymbol{\nabla}\cdot\left(\mathbf{v}\frac{P}{\rho^{\gamma-1}}\right)=0. \tag{2}$$

It is important to realize that the entropy density in Eq. (2) is conserved by each parcel of fluid as it moves, unless it passes through a magnetosonic shock. Also, realize that the above equation is an advection equation. Thus, as long as we use monotonicity-preserving interpolation of the entropy density and as long as the timestep is limited by the Courant number Eq. (2) will produce a positive entropy density. Since the density is always guaranteed to be positive in higher order Godunov schemes, this ensures that Eq. (2) will allow us to derive a consistent and positive definite value of the pressure whenever it is used. In regions of the computational domain where magnetosonic shocks are present the usual MHD equations in conservative form are used. Also in those regions of the computational domain, where the pressure is large enough, we use the MHD equations in conservative form. In those portions of the computational domain, where shocks are not present and where the pressure is a very small fraction of the total energy, one can selectively use the above equation in conjunction with the MHD equations for mass, momentum, and magnetic field. For $x$-directional variations we have the modified system of conservation laws which we write out below as

$$\frac{\partial}{\partial t}\begin{pmatrix}\rho\\ \rho v\\ \rho v\\ \rho v\\ P\rho^{1-\gamma}\\ B_y\\ B_z\end{pmatrix}+\frac{\partial}{\partial x}\begin{pmatrix}\rho v_x\\ \rho v_x^2+P^*\\ \rho v_x v_y-B_xB_y/4\pi\\ \rho v_x v_z-B_xB_z/4\pi\\ v_xP\rho^{1-\gamma}\\ v_xB_y-v_yB_x\\ v_xB_z-v_zB_x\end{pmatrix}=0, \tag{3}$$

where $P^*=P+(1/8\pi)\mathbf{B}^2-(1/4\pi)B_x^2$. Notice that, because we have written the above equations as conservation laws, we can still use the higher order Godunov methodology to help us solve them. The monotone interpolation needed to obtain higher order spatial accuracy can be done either on the primitive variables or the characteristic variables exactly as it is done for the original method. The difference arises in the Riemann solver that we need to use for Eq. (3). We utilize a linearized Riemann solver since iterative Riemann solvers are impracticable for use in MHD simulation codes. In order to formulate a linearized Riemann solver for the above system we need the left and right eigenvectors in conserved variables of Eq. (3). The orthonormal eigenvectors in the primitive variables for MHD have been derived in Roe and Balsara [4] and here denoted by $\tilde{\ell}$ and $\tilde{r}$. We denote the $i$th left and right eigenvectors in the primitive variables by $\tilde{\ell}_i$ and $\tilde{r}_i$. Then the $i$th left and right eigenvectors in the conserved variables of Eq. (3) above are denoted by $\ell_i$ and $r_i$, respectively. They are given by

$$r_i=\mathbf{A}\tilde{r}_i \tag{4}$$

$$\ell_i=\tilde{\ell}_i\mathbf{B}, \tag{5}$$

where **A** and **B** are given by

$$\mathbf{A} = \begin{pmatrix} 1 & 0 & 0 & 0 & 0 & 0 & 0 \\ v_x & \rho & 0 & 0 & 0 & 0 & 0 \\ v_y & 0 & \rho & 0 & 0 & 0 & 0 \\ v_z & 0 & 0 & \rho & 0 & 0 & 0 \\ -(\gamma-1)P\rho^{2-\gamma} & 0 & 0 & 0 & \rho^{1-\gamma} & 0 & 0 \\ 0 & 0 & 0 & 0 & 0 & 1 & 0 \\ 0 & 0 & 0 & 0 & 0 & 0 & 1 \end{pmatrix} \tag{6}$$

$$\mathbf{B} = \begin{pmatrix} 1 & 0 & 0 & 0 & 0 & 0 & 0 \\ -v_x/\rho & \rho^{-1} & 0 & 0 & 0 & 0 & 0 \\ -v_y/\rho & 0 & \rho^{-1} & 0 & 0 & 0 & 0 \\ -v_z/\rho & 0 & 0 & \rho^{-1} & 0 & 0 & 0 \\ (\gamma-1)P\rho^{-1} & 0 & 0 & 0 & \rho^{\gamma-1} & 0 & 0 \\ 0 & 0 & 0 & 0 & 0 & 1 & 0 \\ 0 & 0 & 0 & 0 & 0 & 0 & 1 \end{pmatrix}. \tag{7}$$

Using these eigenvectors the linearized Riemann solver in the entropy variable, i.e. Eq. (3), is easy to construct and the entropy fix is enforced in a style similar to the one described by Harten and Hyman [5] for linearized Riemann solvers of the general type described by Roe [6]. For MHD a linearized Riemann solver for the equations in conserved form has been described in Balsara [7] and the present Riemann solver in the entropy variables complements that effort. A total variation diminishing (TVD) scheme for numerical MHD which utilizes that the Riemann solver is described in Balsara [8]. It must be mentioned that the Riemann solver in the entropy variables has been designed so that it can successfully treat all MHD discontinuities with the sole exception of magnetosonic shocks. Thus in the ensuing paragraphs we construct a set of switches that allow the underlying structure of the MHD flow to be automatically assessed. Based on the assessment we utilize the different linearized Riemann solvers mentioned above. It is also worth mentioning that we used a linearized Riemann solver for MHD that was based on Roe-type linearization, only because it is the one we are most familiar with. Any other linearized Riemann solver for Eq. (2), such as the linearized Riemann solver of Bell, Colella, and Trangenstein [9], can also be used here. It is also worthwhile to point out that linearized Riemann solvers have been shown to fail in regions of high cavitation. In that case Einfeldt *et al.* [10] have shown that the problem can be cured by using the Einfeldt fix. The same insight carries over to MHD where the same fix can be used.

Our strategy is oriented towards ensuring safety first. Thus we utilize a linearized Riemann solver for the MHD equations in the original conserved variables, i.e. with the total energy equation such as the fifth equation in Eq. (3) at all zone boundaries to construct the fluxes. We also design a sequence of switches in each zone. The first switch, **SW1** is intended to make sure that the pressure is much smaller than the energy. **SW1** is switched on when

$$P_{i,j,k} < \alpha E_{i,j,k}, \tag{8}$$

and it is switched off in all other situations. Here $\alpha$ is typically set to 0.05. We assume we are doing a three-dimensional problem on a uniform grid. We use the subscripts $i, j, k$ to

denote the zone-centered variable in the $i,\ j, k^{\text{th}}$ zone in a three-dimensional code. $\alpha$ should be larger than the discretization error of the numerical scheme, and for the TVD scheme described in Balsara [8], which we have used in all the problems here, this value of $\alpha$ is an amply adequate choice.

The second switch is designed to ensure that we are not in the vicinity of a strong magnetosonic shock or a flow configuration that might develop into such a shock. This is accomplished by ensuring that the local minima and maxima of pressure are not too far apart. Thus our second switch **SW2** is switched on if

$$\begin{aligned} &|P_{i+1,j,k} - P_{i-1,j,k}| + |P_{i,j+1,k} - P_{i,j-1,k}| + |P_{i,j,k+1} - P_{i,j,k-1}| \\ &\quad < \tilde{\beta} \min(P_{i,j,k}, P_{i+1,j,k}, P_{i-1,j,k}, P_{i,j+1,k}, P_{i,j-1,k}, P_{i,j,k+1}, P_{i,j,k-1}) \end{aligned} \tag{9}$$

and it is switched off otherwise. Here we have used $\tilde{\beta} = 0.1$.

The method should not exclude situations where mildly compressive motions may take place, but it should certainly exclude strongly compressive motions. A measure of this can be obtained by comparing the undivided divergence of the velocity to the largest local signal speed. Thus, we have our third switch **SW3** which again is switched on if

$$-\delta \max(C_{i,j,k}, C_{i+1,j,k}, C_{i-1,j,k}, C_{i,j+1,k}, C_{i,j-1,k}, C_{i,j,k+1}, C_{i,j,k-1}) < \Delta x (\boldsymbol{\nabla} \cdot \mathbf{v})_{i,j,k} \tag{10}$$

and is switched off otherwise. Here $\delta = 0.03$ was used by us. We have the auxiliary definitions

$$\begin{aligned} \Delta x (\boldsymbol{\nabla} \cdot \mathbf{v})_{i,j,k} &= (v_{x\,i+1,j,k} - v_{x\,i-1,j,k}) + \Delta x \left( \frac{v_{y\,i,j+1,k} - v_{y\,i,j-1,k}}{\Delta y} \right) \\ &\quad + \Delta x \left( \frac{v_{z\,i,j,k+1} - v_{z\,i,j,k-1}}{\Delta z} \right) \end{aligned} \tag{11}$$

$$C_{i,j,k} = \left( \frac{\gamma P_{i,j,k}}{\rho_{i,j,k}} + \frac{B^2_{i,j,k}}{4\pi \rho_{i,j,k}} \right)^{1/2}. \tag{12}$$

With these switches defined, two alternative strategies become possible. The Riemann solver in conservative variables is always utilized at all zone boundaries. In both strategies for those zone boundaries that abut zones that are flagged by **SW1** we also utilize the Riemann solver for the system given in Eq. (3). The differences in the strategies arise from how we use the switches. For the rest of this paper when we refer to the Riemann solver in conservation variables we will refer to it simply as the Riemann solver. Also for the rest of this paper when we refer to the entropy-based Riemann solver we will be referring to the Riemann solver that pertains to the system given in Eq. (3).

### 2.1. *Strategy 1*

In this strategy we only try to correct situations where the pressure might potentially become negative. Thus, we only work with switch **SW1**. In all those zones that are flagged by **SW1** we update the energy equation using the normal Riemann solver. We also update the entropy density Eq. (2) using the fluxes from the pressure-positive Riemann solver

formulated for the system of equations given in Eq. (3). Should the energy equation produce a negative pressure, we derive the updated pressure from Eq. (2) and use that to form a new total energy which corresponds to a positive pressure. Because the energy equation is used most of the time this will result in a pressure update that is not better in its accuracy than the overall accuracy of the numerical scheme. This is so because for most timesteps and in most zones our pressure is still derived from the subtraction of two large numbers.

### 2.2. *Strategy 2*

Here we try to update the pressure with an accuracy that is better than the discretization accuracy of the numerical scheme. To explain this in a little more detail, in a higher order Godunov scheme the discretization errors made in the temporal update of the total energy are a small fraction of the total energy itself. The discretization errors made in updating the entropy density are a small fraction of the entropy density. But because the plasma $\beta$ is so small the entropy density has a much smaller numerical value than the energy. Thus in absolute terms the errors made in evaluating the pressure when it is evaluated using the entropy density are much smaller than those obtained by using the total energy. But it is only possible to use the entropy density equation when the local flow does not have any magnetosonic shocks in it. The entropy density equation is still valid in regions with entropy wave discontinuities or Alfvénic discontinuities. Switches **SW2** and **SW3**, when they are turned on, indicate that the local flow may have Alfvénic or magnetosonic waves in it, but it does not have magnetosonic shocks. This is so because only magnetosonic waves in MHD are compressive in nature and **SW2** and **SW3** are designed to identify such situations. Thus, we necessarily need to use the full compendium of switches designed above in order to safely bypass the energy update in certain zones. In this strategy for all the zones that have been flagged by **SW1** and **SW2** and **SW3**, we update the entropy density using Eq. (2). From the entropy density we construct the pressure in the zone. The updated total energy in that zone is then obtained by using the momentum equation to construct the zone's kinetic energy density and the induction equation to construct the magnetic energy density and adding these two energies to the zone's thermal energy density, obtained from using Eq. (2) along with the fluid continuity equation. Thus, in such zones the energy fluxes are not used to update the total energy equation. As in Strategy 1, should any zone that is flagged by **SW1** produce a negative pressure we use Eq. (2) to provide a positive pressure to that zone instead. This allows us to update the pressure with the discretization accuracies of Eq. (2) and the continuity equation which is better that the discretization accuracy with which the total energy is updated. This is so because the large number constituted by the plasma's kinetic and magnetic energy densities are eliminated in Eq. (2). Thus the pressure is updated with the discretization accuracy of the thermodynamic variables, i.e. the density and entropy density, which is much smaller than that of the total energy variable. It will be shown in the next section that Strategy 2 is the method of choice.

An interesting point must be noted here. In utilizing Eq. (2) we would give up conservation of energy. However, **SW1** identifies those situations where the discretization error in the pressure update is much smaller than the discretization error in the total energy. Since we only utilize Eq. (2) in those local regions of the flow, where **SW1** has been switched on, we locally violate the conservation of total energy. But, because of **SW1** we only violate it in local regions by an amount that is smaller than the discretization accuracy of the total energy equation itself. Besides, because of **SW2** and **SW3** we only violate it in regions of

the flow that are free of magnetosonic shocks. In such regions the importance of energy conservation is minimal. In return, we do get a numerically consistent and positive pressure which maintains greater consistency with the physics in the problem.

## 3. NUMERICAL RESULTS

### 3.1. *Propagation of a Torsional Alfvén Wave Pulse*

As an example we consider the propagation of a torsional Alfvén wave pulse at high speed with respect to the computing grid. The problem is one-dimensional and is set up with 800 zones in the interval $[-0.5, 0.5]$. A fluid with unit density and a pressure of $10^{-2}$ is set up. A uniform $x$-velocity of 10 is given to the fluid in the $x$-direction which is also the direction in which the problem is solved. The magnetic field in the $x$-direction is given a value of 10. The transverse velocities and magnetic fields are denoted by a subscript $T$ and are given below by the formulae

$$\phi = \frac{\pi}{8}[\tanh((x + 0.25)/\delta) + 1][\tanh((0.25 - x)/\delta) + 1] \tag{13}$$

$$\mathbf{V}_T = 10(\cos(\phi)\hat{y} + \sin(\phi)\hat{z}) \tag{14}$$

$$\mathbf{B}_T = -10\sqrt{4\pi}(\cos(\phi)\hat{y} + \sin(\phi)\hat{z}). \tag{15}$$

The pulse is initially set up in the center of the computing grid. Periodic boundaries are assumed. The pulse is allowed to go around the computational domain twice and the simulation is stopped at a time of 0.156. In all the simulations shown below a Courant number of 0.8 was used. This test problem was chosen because the pressure is very small compared to the total energy. In this problem it is less than a ten-thousandth of the total energy in the flow. The pressure is also very small, compared to either the magnetic or kinetic energies. The existence of a strong torsional Alfvén wave discontinuity makes the problem nontrivial. After two passages around the computational domain successful numerical treatment would be indicated by the fact that the pulse's shape is properly preserved. Because the pressure is so small most numerical schemes would produce a negative pressure in some of the zones.

In Figs. 1a–g we show the density, pressure, $x$, $y$, and $z$-velocities and $y$ and $z$-magnetic fields for this problem at the final computational time. The problem was done using Strategy 1. We set $\delta = 0.005$. Figures 2a–g show similar results obtained by using Strategy 1 with $\delta = 0.00125$. Figures 3a–g show the results obtained using Strategy 2 with $\delta = 0.00125$.

We see from Fig. 1b that the pressure has remained positive throughout the course of the simulation. Thus, if the purpose is simply to produce a simulation strategy that never produces negative pressures then we may conclude that Strategy 1 has indeed worked. But we also see from Fig. 1b that the pressure has grown substantially in the course of the simulation. In fact, the pressure has grown to the point where it is approximately of order unity. It must be pointed out that this is about $10^{-2}$ times the total energy in the flow. This is not surprising because schemes of this sort can maintain accuracies of about one part in a hundred at strong discontinuities like the ones we have in our Alfvén pulse. It is just the smallness of the initial pressure distribution that makes this error stand out in our example. This was, in fact, the point of constructing this example. We should note though that this accuracy does not scale as the resolution is improved, because it is determined by the

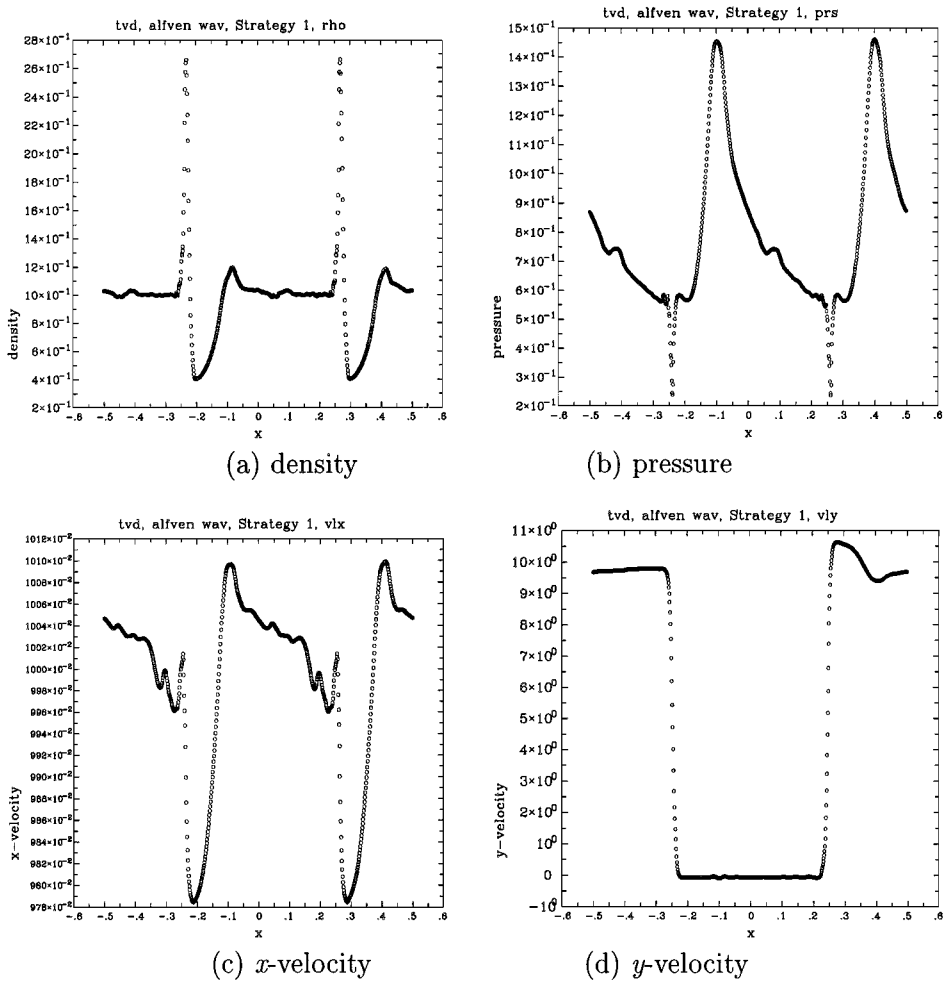


**FIG. 1.** Test problem for a torsional Alfvén wave pulse as described by Eqs. (13)–(15). Here $\delta = 0.005$ at a time of 0.156. Strategy 1 was used.

numerical scheme's ability to handle discontinuities. At discontinuities the interpolation, being monotonicity preserving, produces mostly flat profiles. Thus the accuracy with which such discontinuities can be handled is determined by the Riemann solver. Approximate Riemann solvers always use an average state that is not necessarily representative of the exact discontinuity they have to model. This further degrades the process of capturing discontinuities. The fact that the pressure has increased at the expense of the kinetic and magnetic energies implies that the Riemann solver, whose purpose is to produce stability by selectively introducing dissipation, is doing what it is expected to do. The only problem here is that in doing so it has substantially degraded the quality of the solution; i.e., the Riemann solver has not been selective enough! That point becomes even clearer when viewing the transverse velocities in Figs. 1d and 1e and the transverse magnetic fields in Figs. 1f and 1g. It becomes very clear that the Riemann solver has tried to introduce tiny shocklets into the flow and, given enough time, they have propagated through the computational domain and raised the fluid's entropy and thereby its pressure. The degradation in the fluid's transverse velocity profile is in fact seen to be substantial. Figure 1c for the fluid's $x$-velocity also

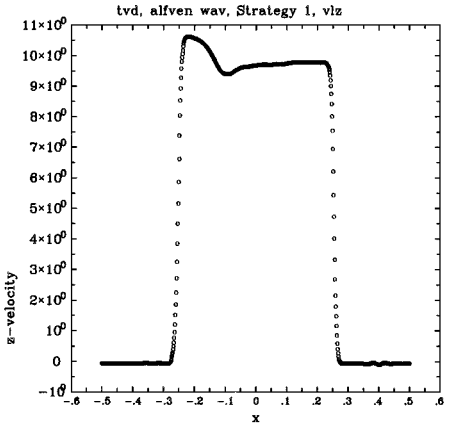


(e) $z$-velocity

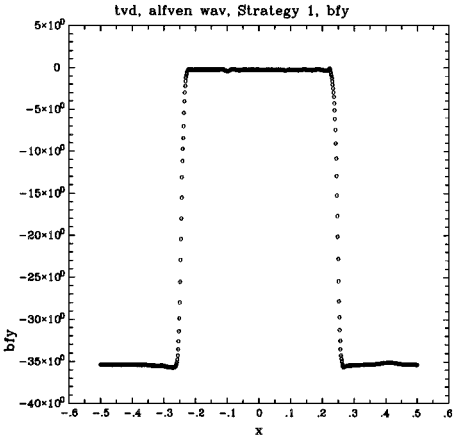


(f) $y$-component of the magnetic field

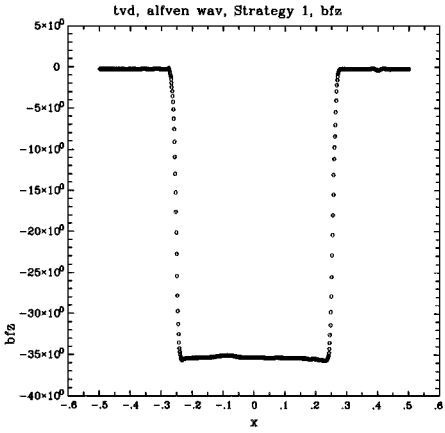


(g) $z$-component of the magnetic field

**FIG. 1**—*Continued*

shows that there have been about 1–2% changes in the $x$-velocity and that is comparable in magnitude to the amount by which the pressure has changed. In fact, one can make an order of magnitude estimate of the kinetic energy to show that a 2% change in a velocity of 10 can cause a change in the pressure that is large enough in our example to bring the pressure's mean magnitude up to unity.

Figure 2 shows that on making the profile narrower the trends noted in the previous paragraph have increased. This is in fact as expected. Owing to the sharpness of the discontinuity the Riemann solver introduces more dissipation faster. Figures 1 and 2 collectively show that the overall goal of producing a simulation which always produces positive pressures can be met. But the price one pays is that the pressure is increased to the point where it is comparable in magnitude to the discretization error of the numerical scheme at strong discontinuities. This is consistent with the explanations given for Strategy 1 in the previous section. An insight that one derives from the above discussion is that Strategy 1 does effectively invoke the entropy-based Riemann solver in order to save the simulation from generating negative pressures. But it invokes the entropy-based Riemann solver too late. Small errors that have accumulated over several timesteps have

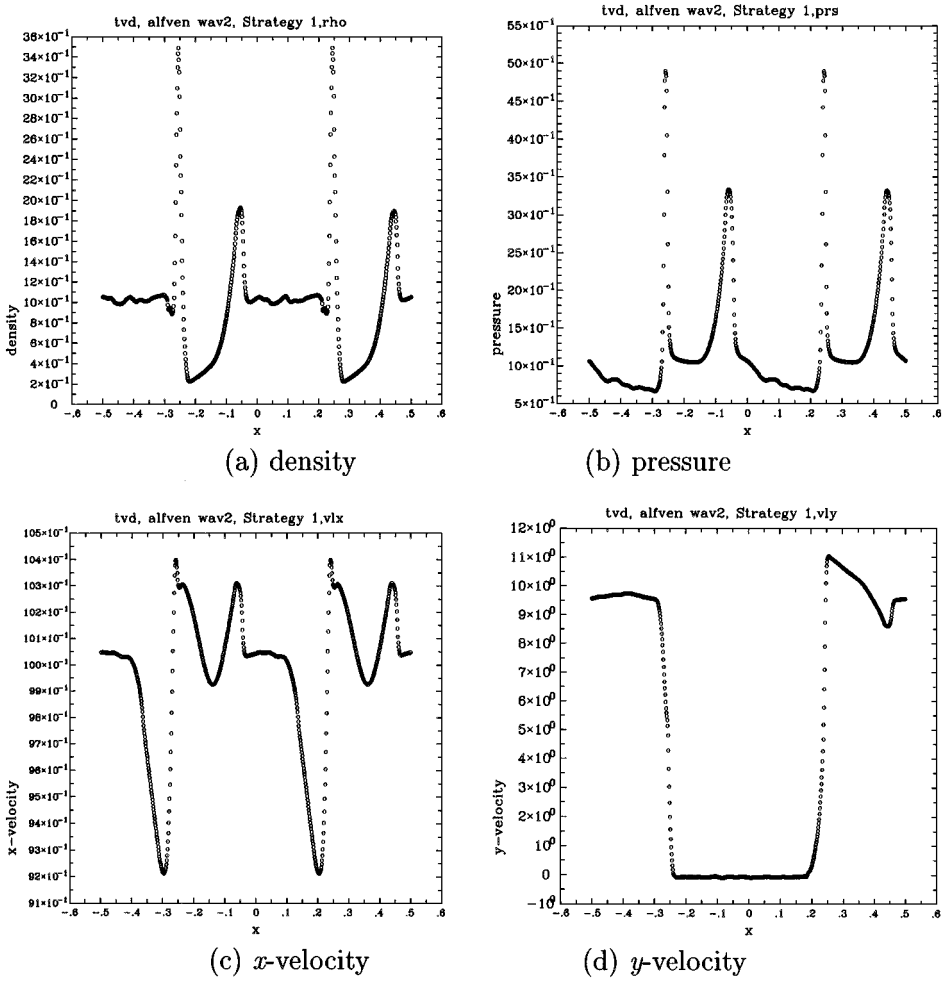


**FIG. 2.** Test problem for a torsional Alfvén wave pulse as described by Eqs. (13)–(15). Here $\delta = 0.00125$ at a time of 0.156. Strategy 1 was used.

already produced large changes in the very small initial pressure field in this problem and by the time the entropy-based Riemann solver is invoked in Strategy 1 the quality of the solution has already been spoiled. Thus, we want to explore how Strategy 2 can rectify that.

Figure 3 shows the solution to the same problem as in Fig. 2. This time the problem was run using Strategy 2. The initial discontinuity in the Alfvén pulse is very sharp and of the order of magnitude of a few zones. Now we see that the pressure has been retained at about the same magnitude as the one we started with. As an added advantage the transverse velocities show sharp, unspoiled profiles. The same is true for the transverse magnetic fields. This shows that the combination of switches that we have used in Strategy 2 have done the job of stepping in and preventing the flow from being degraded. The new entropy-based Riemann solver developed here is invoked as desired and prevents large errors from building up in the pressure variable.

It is also possible to set a floor value for the pressure. In that case one would poll each zone at each timestep to make sure that the floor value was not crossed. Should it be crossed in a particular zone one might arbitrarily raise the pressure in that zone. We have also tried

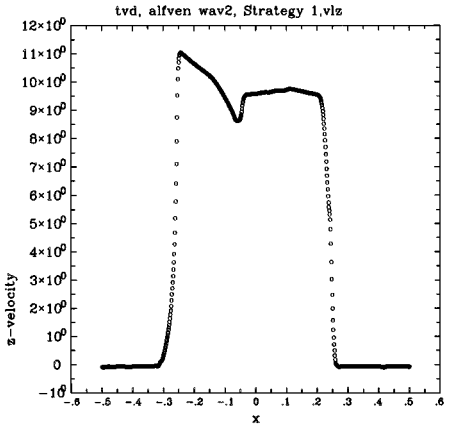


(e) $z$-velocity

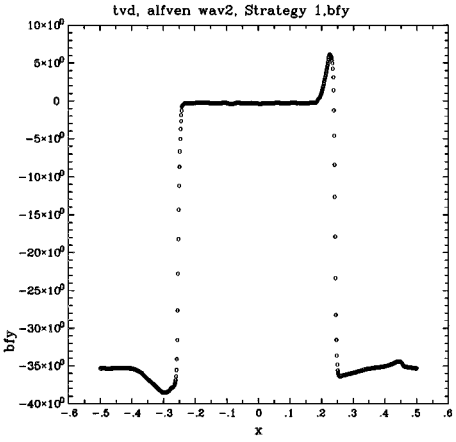


(f) $y$-component of the magnetic field

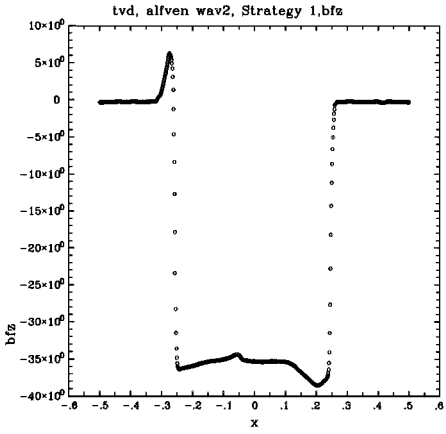


(g) $z$-component of the magnetic field

**FIG. 2**—*Continued*

such a strategy. With judicious choices of the pressure floor value we have been able to obtain solutions that are comparable in quality to those obtained from Strategy 1 but not Strategy 2. There are two fundamental problems with doing that. First, for each problems one has to go through a trial and error process in order to find a good value for the pressure floor. Second, in certain problems with a complex enough flow it may not be possible to find a single floor value that is uniformly applicable to the entire computational domain. We have also carried out simulations involving strong shocks moving through low pressure fluid and found that the strategy designed here successfully switches itself off in the vicinity of shocks.

### 3.2. *Interaction of Alfvén Waves with a Magnetosonic Shock*

In Section 2 we pointed out that the switches were designed to be universal and robust. A key concern for the alert reader may well be that in localized regions of the plasma with low values of $\beta$, when the switches indicate that the flow does not have a magnetosonic shock in the vicinity of a computational zone, we advocate the utilization of Eq. (3)

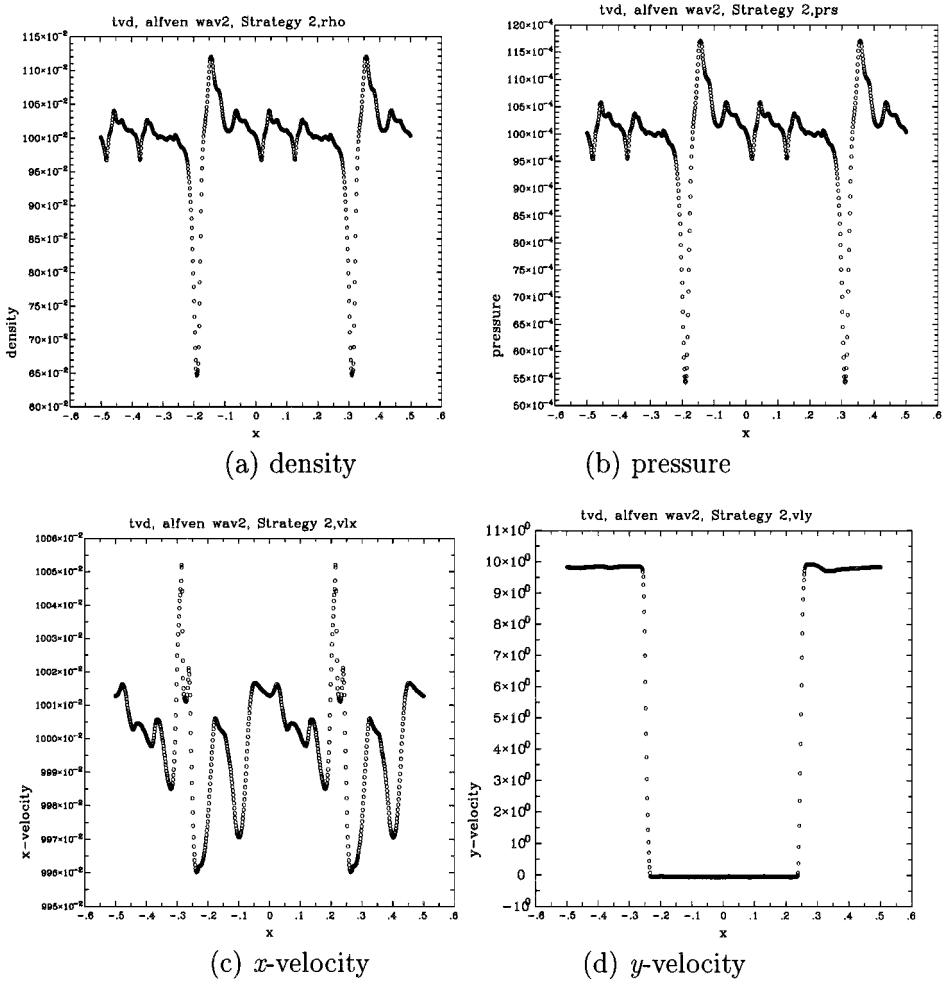


**FIG. 3.** Test problem for a torsional Alfvén wave pulse as described by Eqs. (13)–(15). Here $\delta = 0.00125$ at a time of 0.156.

for the time-update. Thus in order to demonstrate the universality and robustness of the switches we show that when a strong shock interacts with a region of the flow that has a low $\beta$ the result of the simulation is indistinguishable from the result from a corresponding simulation that utilizes a conservation form for the energy equation. The test problem we present was motivated by a hydrodynamical test problem that was presented in Shu and Osher [11]. One possible MHD analogue of that test problem consists of the interaction of a right-going Mach 5 shock with a left-going Alfvén wave that is propagating towards the shock. The Alfvén wave propagates through the preshocked gas which is taken to be a low $\beta$ plasma. Thus in the vicinity of the shock, if the switches are to operate effectively, they should switch back to a form that conserves total energy. The example that we describe in detail in the next paragraph shows that the switches do indeed operate effectively.

The problem is one-dimensional and is set up with 800 zones along the $x$-axis spanning the interval $[-0.5, 0.5]$. The preshocked fluid is at rest and has unit density and a pressure of $10^{-2}$. The preshocked fluid initially occupies the region $[-0.1, 0.5]$. The postshocked

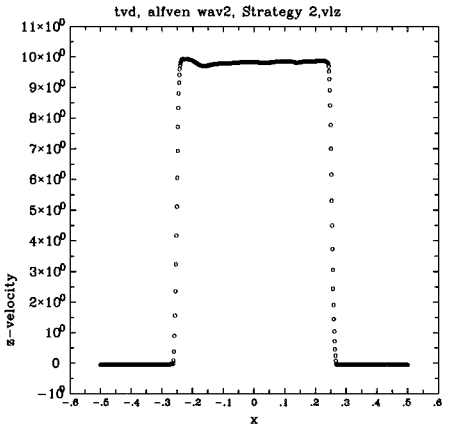


(e) $z$-velocity

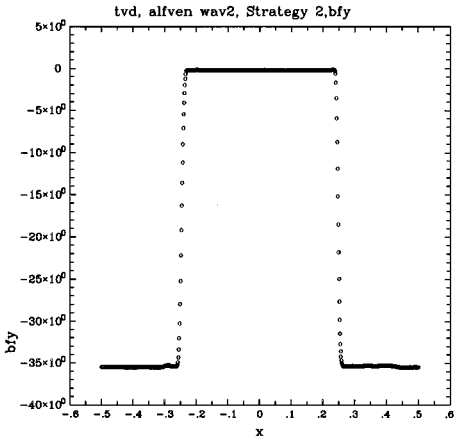


(f) $y$-component of the magnetic field

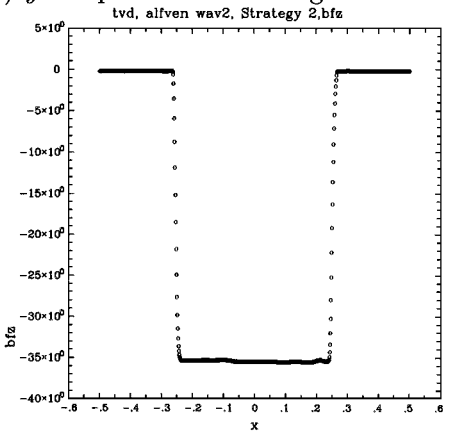


(g) $z$-component of magnetic field

**FIG. 3**—*Continued*

fluid occupies the remaining region and has a density of 5 units, a pressure of 0.28999, and an $x$-velocity of 0.473286. The magnetic field in the $x$-direction has a strength of 10 units. The transverse velocities and magnetic fields in the shocked fluid are set to zero. A left-propagating Alfvén wave is initialized in the unshocked fluid with transverse velocities and magnetic field given by

$$\phi = 2\pi x/\delta \tag{16}$$

$$\mathbf{V}_T = -0.2(\cos(\phi)\hat{y} + \sin(\phi)\hat{z}) \tag{17}$$

$$\mathbf{B}_T = -0.2\sqrt{4\pi}(\cos(\phi)\hat{y} + \sin(\phi)\hat{z}). \tag{18}$$

As the simulation evolved, the ghost zones on the right boundary were given values for the transverse velocity and magnetic field that were consistent with those that are needed to sustain a left-going Alfvén wave. We set $\delta = 1.5$. A Courant number of 0.8 was used. The problem was stopped at a time of 0.2.

In Figs. 4a–g we show the density, pressure, $x$, $y$, and $z$-velocities, and $y$ and $z$-magnetic fields for this problem at the final computational time. The problem was simulated using

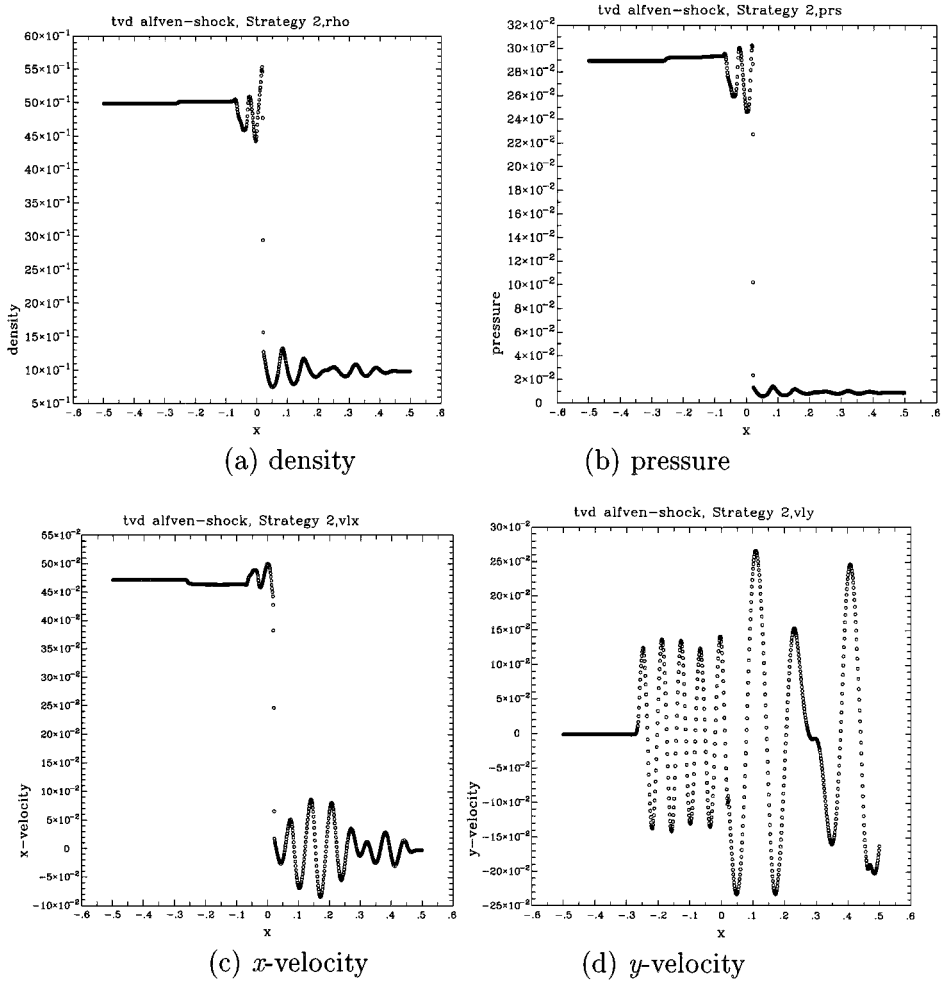


**FIG. 4.** Test problem for the interaction of Alfvén waves with a magnetosonic shock as described by Eqs. (16)–(18) at a time of 0.2.

Strategy 2. We see from Fig. 4 that the Alfvén wave has propagated into the shock, thereby perturbing it. Because the Alfvén wave has a nontrivial strength the perturbations to the magnetosonic shock are substantial. The shock front responds to this perturbation by launching right-going and left-going magnetosonic waves. The density and pressure variables show that by the final time in the simulation the waves have reached the right boundary. The plots for the transverse velocities and magnetic fields show that a portion of the Alfvén wave propagates to the left of the shock. In the unshocked fluid the transverse velocities and magnetic field fluctuations in the right-going magnetosonic waves interact with the corresponding variables in the left-going Alfvén wave. This results in a complex superposition of sinusoids for the transverse velocities and magnetic field in the unshocked gas. The problem was run again without any of the pressure positivity switches. The results were seen to be identical with those in Fig. 4. This demonstrates that the switches do operate effectively and robustly and do not damage the flow by invoking the use of Eq. (3) in regions of the flow where its use is not justified.

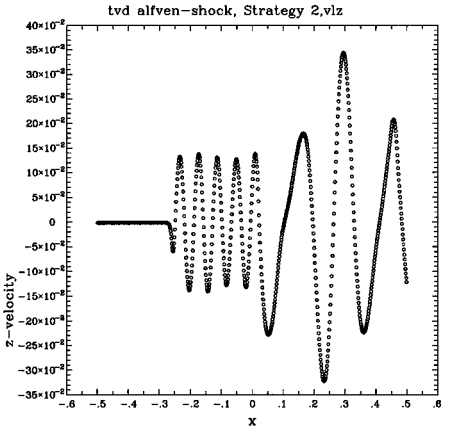


(e) $z$-velocity

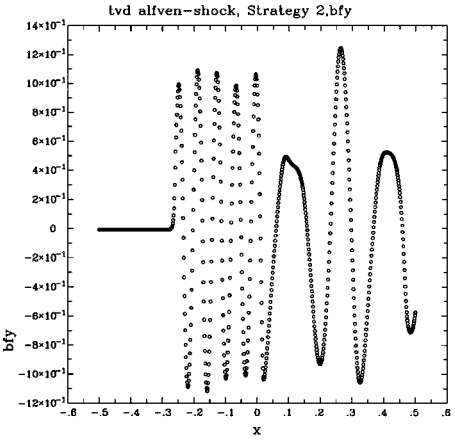


(f) $y$-component of the magnetic field

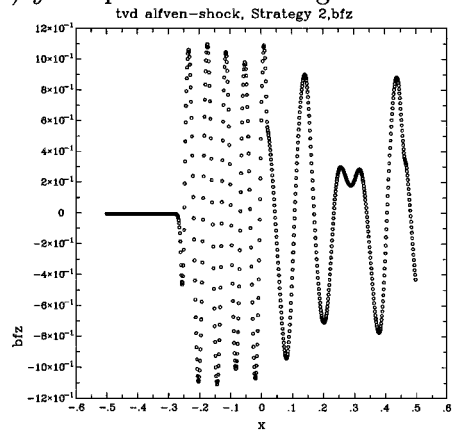


(g) $z$-component of magnetic field

**FIG. 4**—*Continued*

## 4. CONCLUSIONS

In this paper we have constructed strategies for ensuring the positivity of the pressure variable. They are applicable when performing MHD simulations using higher order Godunov schemes. They become especially relevant when the pressure is a very small fraction of the kinetic energy or the magnetic energy. We have constructed two strategies to ensure the positivity of pressure. Strategy 1 does this but is not selective enough to allow us to evolve the pressure variable with small discretization errors, i.e. discretization errors that are much smaller than the overall discretization error of the numerical scheme itself. By constructing numerical examples we show that this is a consequence of Strategy 1 not being selective enough in how it invokes the entropy-based Riemann solver. Strategy 2, by contrast, is shown to be discriminating enough. It allows us to evolve the pressure with an accuracy that scales as the pressure variable itself and is far smaller than the accuracy with which the rest of the equations are evolved. We make this point with an example. Strategy 2 is thus shown to be the method of choice.

It also helps to build one's perspective by comparing the method of Linde and Roe [2] for maintaining pressure positivity and the method developed in Ryu *et al.* [1] and ourselves in

this paper. In the former method one locally reduces the order of accuracy to get pressure positivity. In doing so the Riemann solver's ability to produce local dissipation is in fact utilized. There is a strong tie that the method of Linde and Roe [2], therefore, has to the form of the monotonicity-preserving interpolation that is used. The arithmetic associated with this method also becomes increasingly intractable if interpolation that is better than piecewise linear is used. By contrast the latter method seeks to locally improve on the accuracy, even to the point of trying to update the entropy density with an accuracy that is better than that of the rest of the equations. The normal Riemann solver in the conserved variables is then viewed as being too undiscriminating in how it introduces dissipation. Thus, an attempt is made to selectively switch to another entropy-based Riemann solver that is less dissipative. In doing so we have to introduce a reliance on switches that automatically identify the local regions in the flow where it is acceptable to make this switch. No constraints are put on the form of the interpolation that is to be used. In fact as the interpolation accuracy is improved, say by the introduction of a very high order essentially nonoscillatory interpolation scheme, the dependence on the strategies developed here for maintaining pressure positivity can be selectively reduced.

## REFERENCES

1. D. Ryu, J. P. Ostriker, H. Kang, and R. Cen, *Ap. J.* **414**, 1 (1993).
2. T. Linde and P. L. Roe, preprint.
3. B. vanLeer, *J. Comput. Phys.* **32**, 101 (1979).
4. P. L. Roe and D. S. Balsara, *SIAM J. Appl. Math.* **56**, 57 (1996).
5. A. Harten and J. Hyman, *J. Comput. Phys.* **50**, 235 (1983).
6. P. E. Roe, *J. Comput. Phys.* **53**, 357 (1981).
7. D. S. Balsara, *Ap. J. Supp.* **116**, 119 (1998).
8. D. S. Balsara, *Ap. J. Supp.* **116**, 133 (1998).
9. J. B. Bell, P. Colella, and J. A. Trangenstein, *J. Comput. Phys.* **82**, 362 (1989).
10. B. Einfeldt, C. D. Munz, P. L. Roe, and B. Sjogreen, *J. Comput. Phys.* **92**, 273 (1991).
11. C. W. Shu and S. Osher, *J. Comput. Phys.* **87**, 439 (1989).